

See discussions, stats, and author profiles for this publication at: <https://www.researchgate.net/publication/43339892>

Epithelial, Stromal, and Total Corneal Thickness in Keratoconus: Three-Dimensional Display with Artemis Very-High Frequency Digital Ultrasound

Article in *Journal of refractive surgery* (Thorofare, N.J.: 1995) · April 2010

Impact Factor: 3.47 · DOI: 10.3928/1081597X-20100218-01 · Source: PubMed

CITATIONS

63

READS

115

5 authors, including:



Dan Z Reinstein

144 PUBLICATIONS 2,668 CITATIONS

SEE PROFILE



Marine Gobbe

Columbia University

64 PUBLICATIONS 943 CITATIONS

SEE PROFILE



Ronald H Silverman

Columbia University

208 PUBLICATIONS 3,430 CITATIONS

SEE PROFILE



Donald Jackson Coleman

Columbia University

302 PUBLICATIONS 5,963 CITATIONS

SEE PROFILE

Epithelial, Stromal, and Total Corneal Thickness in Keratoconus: Three-dimensional Display With Artemis Very-high Frequency Digital Ultrasound

Dan Z. Reinstein, MD, MA(Cantab), FRCSC, FRCOphth; Marine Gobbe, MST(Optom), PhD;
Timothy J. Archer, MA(Oxon), DipCompSci(Cantab); Ronald H. Silverman, PhD; D. Jackson Coleman, MD

ABSTRACT

PURPOSE: To characterize the epithelial, stromal, and total corneal thickness profile in a population of eyes with keratoconus.

METHODS: Epithelial, stromal, and total corneal thickness profiles were measured in vivo by Artemis very high-frequency (VHF) digital ultrasound scanning (ArcScan, Morrison, Colo) across the central 6- to 10-mm diameter of the cornea on 54 keratoconic eyes. Maps of the average, standard deviation, minimum, maximum, and range of epithelial, stromal, and total corneal thickness were plotted. The average location of the thinnest epithelium, stroma, and total cornea were found. The cross-sectional semi-meridional stromal and total corneal thickness profiles were calculated using annular averaging. The absolute stromal and total corneal thickness progressions relative to the thinnest point were calculated using annular averaging as well as for 8 semi-meridians individually.

RESULTS: The mean corneal vertex epithelial, stromal, and total corneal thicknesses were $45.7 \pm 5.9 \mu\text{m}$, $426.4 \pm 38.5 \mu\text{m}$, and $472.2 \pm 41.4 \mu\text{m}$, respectively. The average epithelial thickness profile showed an epithelial doughnut pattern characterized by localized central thinning surrounded by an annulus of thick epithelium. The thinnest epithelium, stroma, and total cornea were displaced on average by $0.48 \pm 0.66 \text{ mm}$ temporally and $0.32 \pm 0.67 \text{ mm}$ inferiorly, $0.31 \pm 0.45 \text{ mm}$ temporally and $0.54 \pm 0.37 \text{ mm}$ inferiorly, and $0.31 \pm 0.43 \text{ mm}$ temporally and $0.50 \pm 0.35 \text{ mm}$ inferiorly, respectively, with reference to the corneal vertex. The increase in semi-meridional absolute stromal and total corneal thickness progressions was greatest inferiorly and lowest temporally.

CONCLUSIONS: Three-dimensional thickness mapping of the epithelial, stromal, and total corneal thickness profiles characterized thickness changes associated with keratoconus and may help in early diagnosis of keratoconus. [*J Refract Surg.* 2009;xx:xxx-xxx.] DOI:1.9999/1081597X-200905015-06

Keratoconus is a non-inflammatory corneal disease characterized by a cone-like-shaped protrusion of the corneal surface. It is associated with progressive corneal thinning, steepening of corneal curvature, and irregular astigmatism, resulting in mild to marked impaired quality of vision. It is a bilateral but often asymmetric disorder.

Total corneal thickness changes associated with keratoconus are due to changes in both stromal thickness and epithelial thickness. Although central total corneal thickness and total corneal thickness profile have been widely reported, only a limited number of studies have reported central stromal or epithelial thickness, and there are no published studies showing pachymetric maps of the stroma or epithelium.

Central corneal thinning in keratoconus has been reported using different methods such as ultrasound pachymetry,¹⁻⁶ Orbscan (Bausch & Lomb, Salt Lake City, Utah),^{2,5-8} Pentacam (Oculus Optikgeräte, Wetzlar, Germany),^{4,9,10} specular microscopy,⁶ ultrasound biomicroscopy,^{11,12} and optical coherence tomography (OCT).^{5,13} Total corneal thickness profile in kera-

From London Vision Clinic, London, United Kingdom (Reinstein, Gobbe, Archer); Department of Ophthalmology, St Thomas' Hospital - Kings College, London, United Kingdom (Reinstein); the Department of Ophthalmology, Weill Medical College of Cornell University, NY (Reinstein, Silverman, Coleman); Centre Hospitalier National d'Ophthalmologie, Paris, France (Reinstein) and Riverside Research Institute, New York, NY, (Silverman).

Supported in part by NIH grant EB000238 and the Dyson Foundation, Millbrook, NY.

Drs Reinstein, Silverman, and Coleman have a proprietary interest in the Artemis technology (ArcScan Inc, Morrison, Colo) and are the authors of patents related to VHF digital ultrasound administered by the Cornell Center for Technology Enterprise and Commercialization (CCTEC), Ithaca, NY. The remaining authors have no proprietary or financial interest in the materials presented herein.

Preparation in part fulfillment of the requirements for the doctoral thesis, University of Cambridge, for Dr Reinstein.

Some of the aspects of this study were presented at the American Academy of Ophthalmology Annual Meeting; November 15-18, 2003; Anaheim, Calif.

Correspondence: Dan Z. Reinstein, MD, MA(Cantab), FRCSC, FRCOphth, London Vision Clinic, 8 Devonshire Pl, London W1G 6HP, United Kingdom. Tel: 44 207 224 1005; Fax: 44 207 224 1055; E-mail: dzt@londonvisionclinic.com

Received: December 15, 2008; Accepted: April 14, 2009

toconus has been measured previously using Orbscan,⁷ Pentacam,^{9,10,14} and Visante OCT (Carl Zeiss Meditec AG, Jena, Germany)¹⁵ whereas other studies have provided total corneal thickness measurements at specific locations in the peripheral cornea.^{1,3,5,12,16-18}

In keratoconus, the epithelium is known to thin in the area overlying the cone, and in advanced keratoconus, there may be excessive epithelial thinning leading to a breakdown in the epithelium. Epithelial thinning over the cone has been demonstrated using histopathologic analysis of keratoconic corneas,¹⁹ and the central epithelial thickness was found to be thinner in keratoconus than in normal corneas using OCT.⁵ Transmission electron microscopy has demonstrated that the epithelial thickness was irregular in keratoconus.²⁰

The stromal thickness profile is also of interest to study as stromal thinning occurs during the progression of the disease.^{5,21} Early changes in the stromal thickness progression may be helpful in the early diagnosis of keratoconus.

Artemis very high-frequency (VHF) digital ultrasound (ArcScan, Morrison, Colo) is to date the only published method of accurately measuring individual corneal layers, including the epithelium and stroma, continuously over a large area.^{22,23} We have previously used the Artemis to describe the average epithelial thickness profile²⁴ and stromal thickness profile²⁵ in a population of normal eyes. The repeatability of total corneal thickness measurements in 10 consecutive examinations of 1 eye using the Artemis 1 VHF digital ultrasound arc-scanning system has been shown to be less than 8 μm within the central 8-mm diameter, with a central repeatability of 1.5 μm .²³ The repeatability of epithelial thickness measurements in the normal population has been shown to be less than 1.30 μm within the central 8-mm diameter, with a central repeatability of 0.5 μm .²³

The purpose of this study was to qualitatively and quantitatively characterize the thickness profile of the epithelium, stroma, and full cornea in a population of keratoconic eyes using the Artemis VHF digital ultrasound arc-scanning system.

PATIENTS AND METHODS

PATIENT POPULATION

This study was a retrospective case series collected from a consecutive population of keratoconus patients examined at the London Vision Clinic, London, United Kingdom, between July 2005 and August 2007. A complete ocular examination was performed to confirm the diagnosis of keratoconus. The preoperative assessment of all patients included manifest refraction, log-MAR best spectacle-corrected visual acuity (BSCVA)

(CSV-1000 Vector Vision Inc, Greenville, Ohio), and cycloplegic refraction using one drop of tropicamide 1% (Alcon Laboratories UK, Ltd, Hemel Hempstead, United Kingdom). Tomography was assessed using the Orbscan II and topography and simulated keratometry (K) were assessed using the Atlas corneal topography system (Carl Zeiss Meditec AG). Dynamic pupillometry was carried out using the Procyon P2000 pupillometer (Haag-Streit, Bern, Switzerland). Wavefront assessment was performed using the WASCA aberrometer (Carl Zeiss Meditec AG). Single-point pachymetry was performed with the Corneo-Gage Plus (50 MHz) hand-held ultrasound pachymeter (Sonogage, Cleveland, Ohio) by determining the minimum of 10 consecutive central total corneal measurements. Three-dimensional epithelial, stromal, and total corneal thickness for the central 8- to 10-mm diameter was measured using the Artemis 1 technology.

Patients included for the study met the following inclusion criteria: a) patients previously diagnosed with keratoconus, and b) patients whose diagnosis was confirmed by clinical signs of keratoconus such as microscopic signs at the slit lamp, corneal topographic changes, high refractive astigmatism, reduced BSCVA and contrast sensitivity, and significant level of higher order aberrations, in particular coma. The population included eyes at different stages of the disease, ranging from cases with indisputable keratoconus by topography, but without microscopic signs at the slit-lamp, to extreme cases approaching the need for corneal transplant, demonstrating clear microscopic signs such as Vogt's striae and substantial corneal thinning. In patients where the second eye demonstrated suspected keratoconus (ie, a diagnosis of keratoconus could not be confirmed), the second eye was excluded. Patients with pellucid marginal degeneration were excluded. Patients with apical corneal scarring were also excluded.

Patients gave informed consent for the use of their data for research, analysis, and publication purposes.

ARTEMIS VHF DIGITAL ULTRASOUND ARC-SCANNING

The Artemis VHF digital ultrasound system has been described in detail previously.²⁴ Briefly, Artemis VHF digital ultrasound is carried out using an ultrasonic standoff medium. The patient sits and positions the chin and forehead into a headrest while placing the eye in a soft rimmed eye-cup. Warm sterile normal saline (33°C) is filled into the darkened scanning chamber. The patient fixates on a narrowly focused aiming beam, which is coaxial with the infrared camera, the corneal vertex, and the center of rotation of the scanning system. The technician adjusts the center of rotation of the system until it is coaxial with the cor-

neal vertex. In this manner, the position of each scan plane is maintained about a single point on the cornea and corneal mapping is therefore centered on the corneal vertex. The Artemis VHF digital ultrasound uses a broad band 50 MHz VHF ultrasound transducer (bandwidth approximately 10 to 60 MHz), which is swept by a reverse arc high-precision mechanism to acquire B-scans as arcs that follow the surface contour of anterior or posterior segment structures of interest. Performing a three-dimensional scan set with the Artemis 1 takes approximately 2 to 3 minutes per eye.

Using VHF digital ultrasound, interfaces between tissues are detected at the location of the maximum change in acoustic impedance (the product of the density and the speed of sound). It was first demonstrated in 1993 that acoustic interfaces being detected in the cornea were located spatially at the epithelial surface and at the interface between epithelial cells and the anterior surface of Bowman's layer.²⁶ This indicated that stromal thickness measurement with VHF digital ultrasound includes Bowman's layer. The posterior boundary of the stroma with VHF digital ultrasound is located at the interface between the endothelium and the aqueous, as this is the location of the maximum change in acoustic impedance. This indicated that stromal thickness measurement with VHF digital ultrasound includes Descemet's membrane and the endothelium.

The Artemis 1 scanner described herein is the precursor to the commercially available Artemis 2 (Arc-Scan Inc). The main difference is that the Artemis 1 uses a polyvinylidene fluoride (PVDF) transducer whereas the Artemis 2 uses a lithium niobate transducer (which is more sensitive). Both PVDF and lithium niobate probes produce the same accuracy of measurement, as this varies according to frequency and bandwidth, not sensitivity. The digital signal processing technology and the arc described for anterior segment as well as corneal scanning are identical for both instruments.

THREE-DIMENSIONAL PACHYMETRIC TOPOGRAPHY

For three-dimensional scan sets, the scan sequence consisted of four meridional B-scans at 45° intervals. Each scan sweep takes about 0.25 seconds and consisted of 128 scan lines or pulse echo vectors. Ultrasound data are digitized and stored. The digitized ultrasound data are then transformed using patented Cornell University digital signal processing technology, which includes auto-correlation of back surface curvatures to center and align the meridional scans. A speed of sound constant of 1640 m/s was used.

STATISTICAL ANALYSIS

Descriptive statistics (average, minimum, maximum,

standard deviation, and range) were calculated for each point in the 10×10-mm Cartesian matrix across eyes. These statistics were carried out for all eyes using vertical mirrored symmetry superimposition; thickness values for left eyes were reflected in the vertical axis and superimposed onto the right eye values so that nasal/temporal characteristics could be combined. The resultant matrices were plotted using DeltaGraph v5.0 (SPSS Inc, Richmond, Calif) as surface fill X,Y,Z plots to represent the point-by-point average, standard deviation, minimum, maximum, and range of the population. Qualitative assessment of individual variability within corneas and across the population was performed. Fifteen eyes were chosen at random using Microsoft Excel's (Microsoft Corp, Redmond, Wash) random number function to demonstrate examples of the epithelial thickness profile in keratoconic eyes. The point locations of the thinnest epithelium, thinnest stroma, and thinnest cornea were determined for each eye (using mirrored left eyes) and the average and standard deviation of the x- and y-coordinates of the thinnest point were calculated. The standard deviation of epithelial thickness within the central 3-, 5-, and 7-mm zones was determined for each eye to represent the within-eye variation of epithelial thickness. The average and standard deviation of the within-eye variation were found and the distribution of the within-eye variation was plotted. This analysis was performed so the results could be compared to a similar analysis for a population of normal eyes.²⁴

To quantify the irregularity of the epithelial thickness profile, the values of the thinnest and thickest epithelium were determined for each eye and the difference between the thinnest and thickest point was calculated. Linear regression analysis was performed with the hypothesis that there is a correlation between 1) the thinnest epithelial value of a cornea and the steepest point value for the Atlas keratometric map of the same cornea, 2) the thickest epithelial value of a cornea and the steepest point value for the Atlas keratometric map of the same cornea, and 3) the difference between the thinnest and thickest epithelial values of a cornea and the steepest point value for the Atlas keratometric map of the same cornea. The coefficient of determination (R^2) was calculated for each of these correlations.

The stromal and total corneal thickness data for each eye were transposed to center the data on the thinnest point rather than the corneal vertex. Descriptive statistics (average and standard deviation) were recalculated and mapped for all eyes with the thinnest point as the origin. The cross-sectional semi-meridional average stromal and total corneal thickness profile

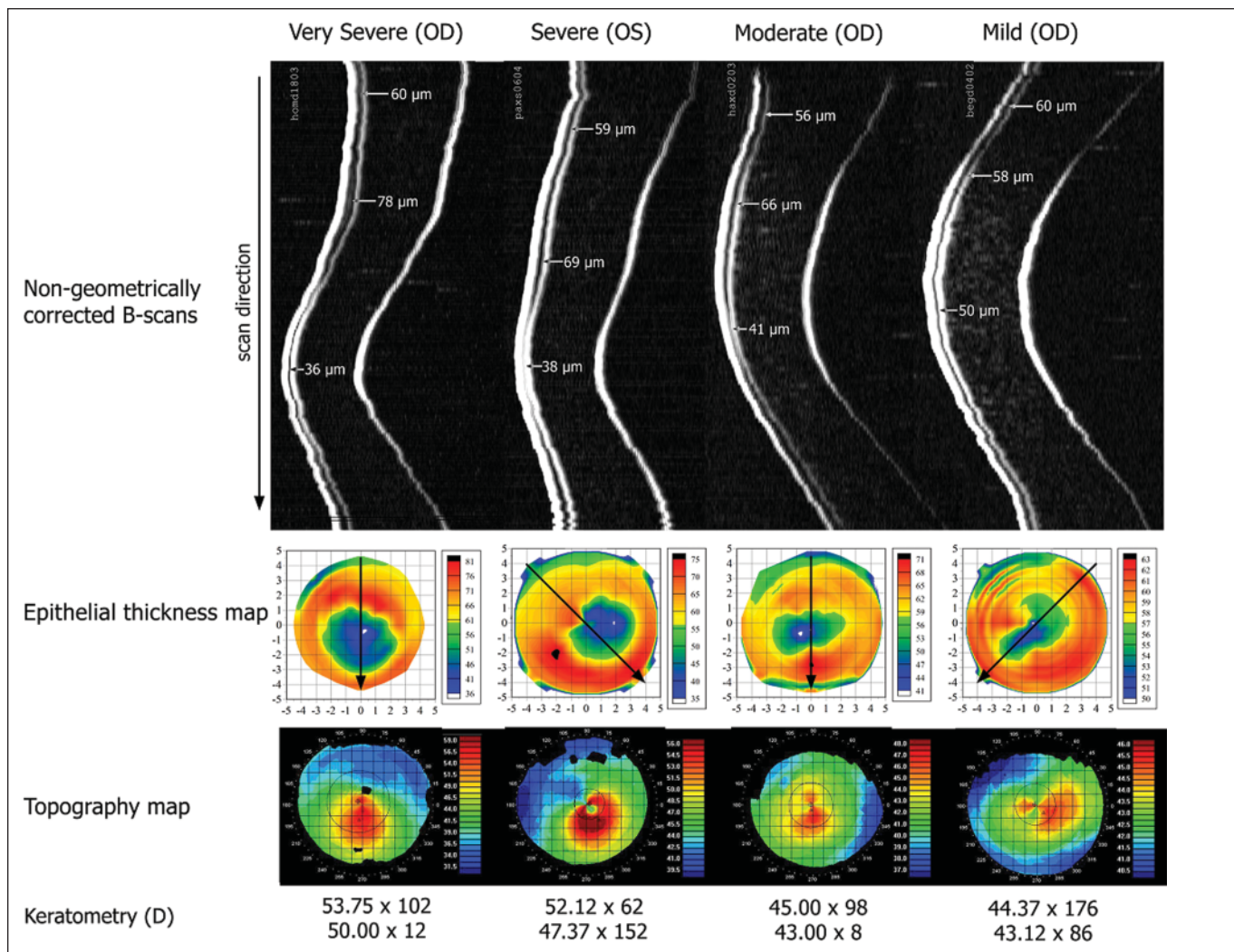


Figure 1. Non-geometrically corrected Artemis B-scan images obtained using the Artemis very high-frequency digital ultrasound arc-scanner, Artemis epithelial thickness profile maps, and Atlas axial curvature maps for four keratoconic corneas at different stages of the disease ranging from severe keratoconus to mild keratoconus.

were determined for each eye by averaging the stromal and total corneal thickness within the 0.03-mm zone centered on the thinnest point and within 35 annular bands each 0.06-mm wide centered on the thinnest point with central radii increasing in 0.1-mm steps. The average stromal and total corneal thicknesses within each annular band were plotted against the radial distance from the thinnest point.

To investigate the absolute stromal thickness progression from the thinnest point towards the periphery, the difference between the stromal thickness for each annular band of each eye and the thinnest stroma in the same eye was calculated. The average of these differences was plotted against the radial distance from the thinnest point. Polynomial linear regression analysis was performed, and the regression equation and the coefficient of determination (R^2) were calculated to de-

scribe the absolute stromal thickness progression from the thinnest point to the periphery. The same analysis was also performed to describe the absolute total corneal thickness progression.

To investigate the symmetry of the absolute stromal thickness progression, directional semi-meridional absolute stromal thickness progression was also calculated. The difference between the stromal thickness and the stroma at the thinnest point was calculated at 0.1-mm steps for eight semi-meridians at 45° intervals: the nasal (0°) and temporal (180°) horizontal meridian, the superior (90°) and inferior (270°) vertical meridian, the superonasal (45°) and inferotemporal (225°) meridian, and the superotemporal (135°) and inferonasal meridian (315°). The average absolute stromal thickness progression was plotted against the radial distance from the thinnest point for each of the eight semi-meridians. The same analysis

TABLE 1

Corneal Vertex Epithelial, Stromal and Total Corneal Thickness in 54 Eyes With Keratoconus

	Thickness (μm)		
	Epithelium	Stroma	Total Cornea
Mean \pm SD	45.7 \pm 5.9	426 \pm 38.5	472 \pm 41.4
95% CI	[44.9-46.5]	[421-438]	[467-478]
Minimum	33.1	312	346
Maximum	56.3	493	546
Range	23.2	181	200

SD = standard deviation, 95% CI = 95% confidence interval

TABLE 2

Epithelial, Stromal, and Total Corneal Thickness at the Thinnest Location in 54 Eyes With Keratoconus

	Thickness (μm)		
	Epithelium	Stroma	Total Cornea
Mean \pm SD	38.2 \pm 5.8	406 \pm 42.1	450 \pm 43.9
Minimum	29.6	298	338
Maximum	52.4	489	540
Range	22.8	191	201

SD = standard deviation

was also performed to describe the symmetry of the absolute total corneal thickness progression.

Descriptive statistics, comparative statistics, and linear regression analysis were performed in Microsoft Excel 2003. A *P* value <.05 was deemed to be significant.

RESULTS

During the study period, 54 eyes (27 right and 27 left eyes) of 30 patients were included for evaluation. There were 6 patients whose other eye was excluded from the study for the following reasons: suspected keratoconus in 3 eyes, corneal graft in 2 eyes, and apical corneal scarring in 1 eye. The population breakdown was 57.4% Caucasian, 25.9% East Indian, 13.0% Black, and 3.7% Arabic. Mean patient age was 29.3 \pm 6.1 years (median: 29.3 years, range: 18.3 to 41.9 years). The mean refraction was -1.45 ± 3.40 diopters (D) sphere (range: -8.25 to $+9.75$ D), and 3.40 \pm 2.51 D cylinder (range: 0.00 to 12.00 D). Mean BSCVA was 0.24 \pm 0.32 logMAR. The mean maximum keratometry was 50.20 \pm 5.80 D (range: 42.20 to 63.50 D). The mean minimum keratometry was 45.50 \pm 3.60 D (range: 39.80 to 53.70 D).

B-SCAN

Figure 1 shows non-geometrically corrected Artemis B-scan images, Artemis epithelial thickness profile maps, and Atlas axial curvature maps for four keratoconic corneas at different stages of the disease ranging from severe keratoconus to mild keratoconus. The protrusion of the cone on the back surface of the cornea as well as on the front surface of the cornea can be clearly seen on the B-scans, with the cone more apparent as the severity of the keratoconus increases. The B-scans also demonstrate central total corneal thinning, which is more evident in the more severe cases of keratoconus. The lack of homogeneity in epithelial thickness characterized by thinner epithelial over the cone with

thicker epithelium adjacent to the cone is also visible on the B-scans. The thin epithelium at the apex of the cone as well as the thicker epithelium bordering the cone is clearly visible for the two most severe cases, still visible for the moderate case although less pronounced, but hardly noticeable for the mild case. However, the epithelial thickness profile map clearly demonstrates a similar pattern of thin central epithelium and surrounding thicker epithelium.

EPIHELIAL PACHYMETRIC TOPOGRAPHY

Table 1 presents statistical data for the corneal vertex epithelial thickness for all eyes.

The average epithelial thickness map (Fig 2, row 1, column 1) showed an epithelial doughnut pattern, characterized by a localized central zone of thinning surrounded by an annulus of thick epithelium. The epithelial doughnut pattern was slightly decentered inferotemporally.

Analysis of the thinnest epithelial point (Fig 3) revealed that the mean thinnest epithelial point was displaced 0.48 \pm 0.66 mm temporally and 0.32 \pm 0.67 mm inferiorly with reference to the corneal vertex. The thinnest epithelial point was located in the inferotemporal quadrant for 74% of eyes (40/54), in the superotemporal quadrant in 16.7% of eyes (9/54), in the superonasal quadrant for 1.9% eyes (1/54), and in the inferonasal quadrant in 7.4% of eyes (4/54). Table 2 presents statistical data for the thinnest epithelial point. The epithelium at the thinnest point was on average 7.5 μm thinner than at the corneal vertex, which was a statistically significant difference (*P*<.001).

Analysis of the thickest epithelial point revealed that the mean thickest epithelial point was displaced 0.10 \pm 1.18 mm nasally and 0.92 \pm 1.65 mm inferiorly with reference to the corneal vertex. The mean thickest epithelium for all eyes was 66.8 \pm 7.2 μm (range: 54.1

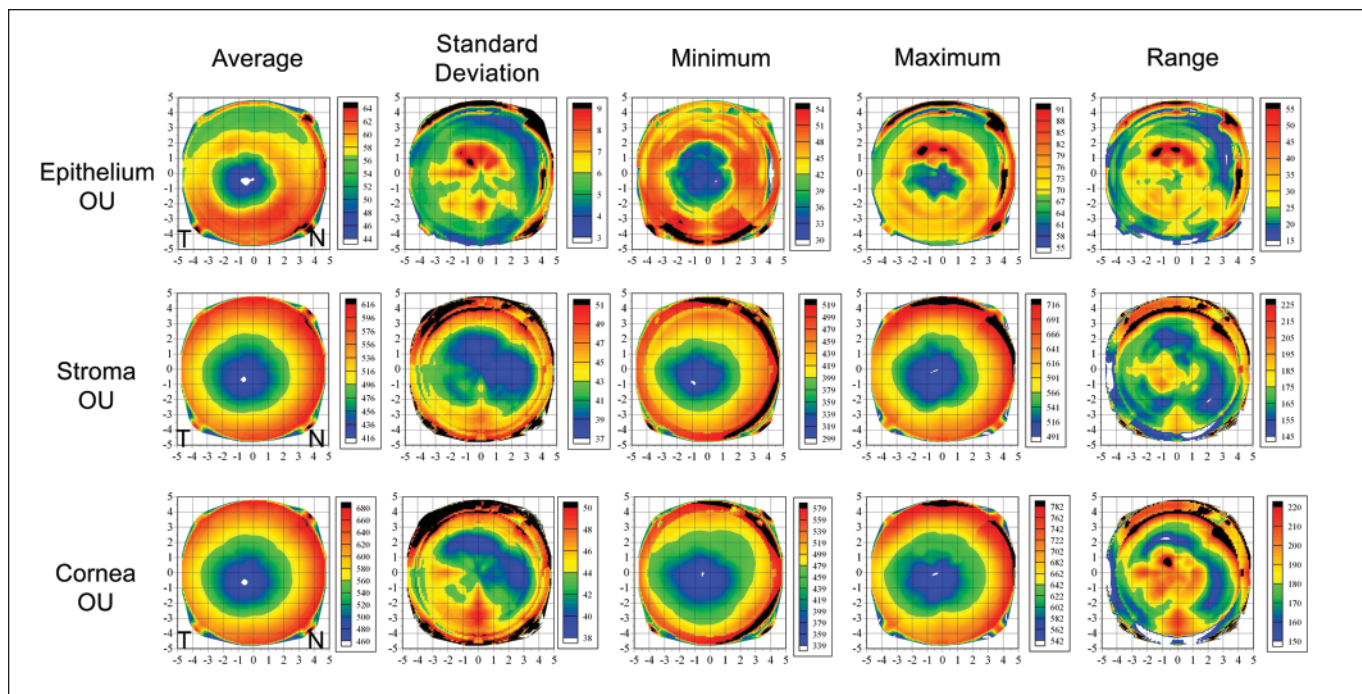


Figure 2. Topographical map of the descriptive statistics of epithelial thickness, stromal thickness, and total corneal thickness centered on the corneal vertex for the population. All eyes are included with left eyes mirrored (positive values represent the nasal cornea and negative values represent the temporal cornea). The color scale represents the thickness in microns. A Cartesian 1-mm grid is superimposed with the origin at the corneal vertex.

to 94.4 μm). The mean difference between the thinnest and thickest epithelium was 28.6 ± 10.8 μm (range: 5.1 to 59.1 μm).

Figure 4 shows the epithelial thickness profile for 15 eyes of the population selected at random using Microsoft Excel’s random number function. Although all eyes exhibited the same epithelial doughnut pattern, the thickness values of the thinnest epithelium and thickest epithelium, as well as the difference in thickness between the thinnest and thickest epithelium, varied greatly in the population. For example, case 12 shows a minimum epithelial thickness of 47 μm, and a difference of 14 μm between the thinnest and thickest epithelium. In contrast, case 15 shows a minimum epithelial thickness of 33 μm, and a difference of 45 μm between the thinnest and thickest epithelium.

A statistically significant and relatively strong correlation ($R^2=0.47, P<.05$) was noted between the steepest keratometry and the thinnest epithelium in the central zone of the epithelial doughnut pattern (Fig 5A), indicating that the minimum epithelial thickness was thinner in eyes with steeper keratometry, suggesting there is more epithelial thinning in the central zone of the epithelial doughnut pattern in advanced cases of keratoconus where the cone is more pronounced. There was also a statistically significant correlation ($R^2=0.29, P<.05$) between the steepest keratometry and the thickest epithelium (Fig 5B). This indicated that the maxi-

imum epithelial thickness was greater in eyes with steeper keratometry, suggesting there is more epithelial thickening in the annular zone of the epithelial doughnut pattern in advanced cases of keratoconus where the cone is more pronounced. Following on from these two results, there was a statistically significant correlation ($R^2=0.53, P<.05$) between the steepest keratometry and the difference between the thinnest and thickest epithelium within the epithelial doughnut pattern (Fig 5C).

The map of epithelial thickness standard deviation (see Fig 2, row 1, column 2) showed more variation in epithelial thickness in the central cornea. The nasal, superior, and inferior peripheral regions demonstrated the least variation. The map of the minimum epithelial thickness (see Fig 2, row 1, column 3) demonstrated the thinnest epithelium within the study population to be within the central 1-mm diameter zone. The thinnest central epithelium was 30 μm, whereas the thinnest inferior epithelium was 57 μm. The map of the maximum epithelial thickness (see Fig 2, row 1, column 4) showed that the thickest epithelium in the study population was found in the mid-peripheral zone surrounding the thin epithelium. The thickest epithelium was 94 μm located 1.5-mm superior of the corneal vertex whereas the thickest epithelium at the corneal vertex was only 55 μm. The map of the range of epithelial thicknesses (see Fig 2, row 1, column 5) showed that the largest range in epithelial thickness in the study

population was found in the annular region of epithelial thickening surrounding the thin epithelium. The smallest range of epithelial thickness was found in the peripheral cornea, in the superonasal area.

The mean within-eye variation of epithelial thickness for the central 3-, 5-, and 7-mm diameter zones remained similar as the analysis zone diameter increased (Fig 6)— $6.51 \pm 3.31 \mu\text{m}$ for the central 3 mm, $7.02 \pm 3.29 \mu\text{m}$ for the central 5 mm, and $6.37 \pm 2.70 \mu\text{m}$ for the central 7 mm.

STROMAL AND TOTAL CORNEAL PACHYMETRIC TOPOGRAPHY

Table 1 presents statistical data for the corneal vertex stromal and total corneal thickness.

The average stromal thickness map (see Fig 2, row 2, column 1) and the average total corneal thickness map (see Fig 2, row 3, column 1) showed as expected that the stroma and the total cornea were thinner centrally and became increasingly thicker towards the peripheral cornea.

Analysis of the thinnest point location (see Fig 3) revealed that for most eyes, the thinnest stromal and total corneal points were displaced inferotemporally with reference to the corneal vertex for both the stroma and cornea. The mean location of the thinnest stromal point was displaced $0.38 \pm 0.42 \text{ mm}$ temporally and $0.57 \pm 0.36 \text{ mm}$ inferiorly with reference to

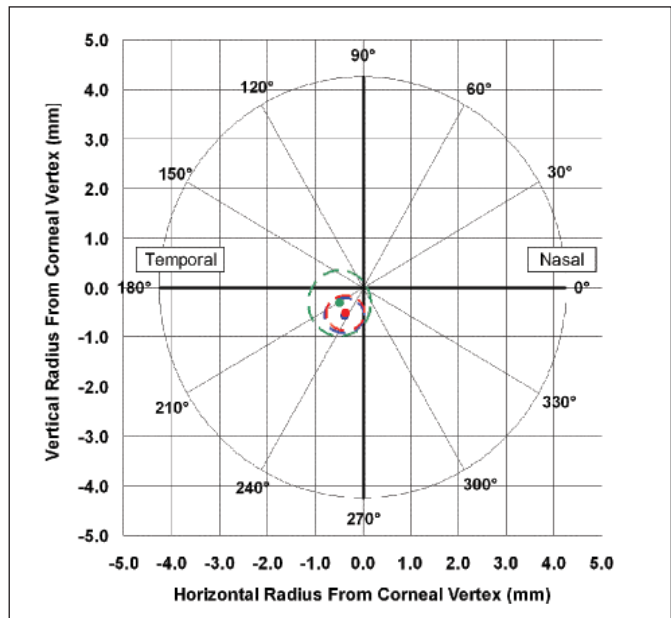


Figure 3. Average location of the thinnest epithelium, thinnest stroma, and thinnest total cornea within the central 5 mm of the cornea. The dots represent the average location of the thinnest point for all eyes tested, and the ellipses represent one standard deviation in the x- and y-directions. The epithelium is represented in green, the stroma in blue, and the total cornea in red. A Cartesian 1-mm grid is superimposed with the origin at the corneal vertex. Positive x values represent the nasal cornea and negative values represent the temporal cornea. Positive y values represent the superior cornea and negative values represent the inferior cornea.

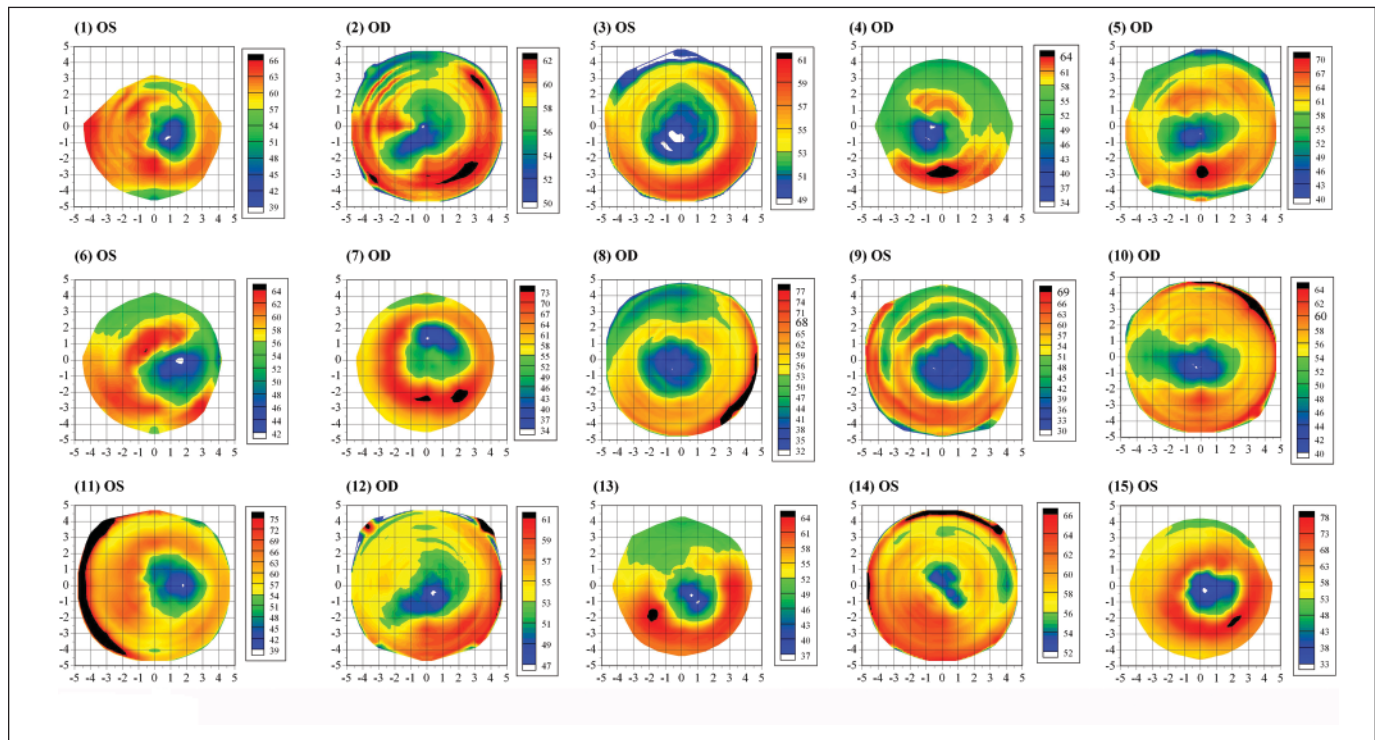


Figure 4. Epithelial thickness maps of 15 randomly selected eyes each plotted with an individual color scale representing the epithelial thickness in microns. A Cartesian 1-mm grid is superimposed with the origin at the corneal vertex.

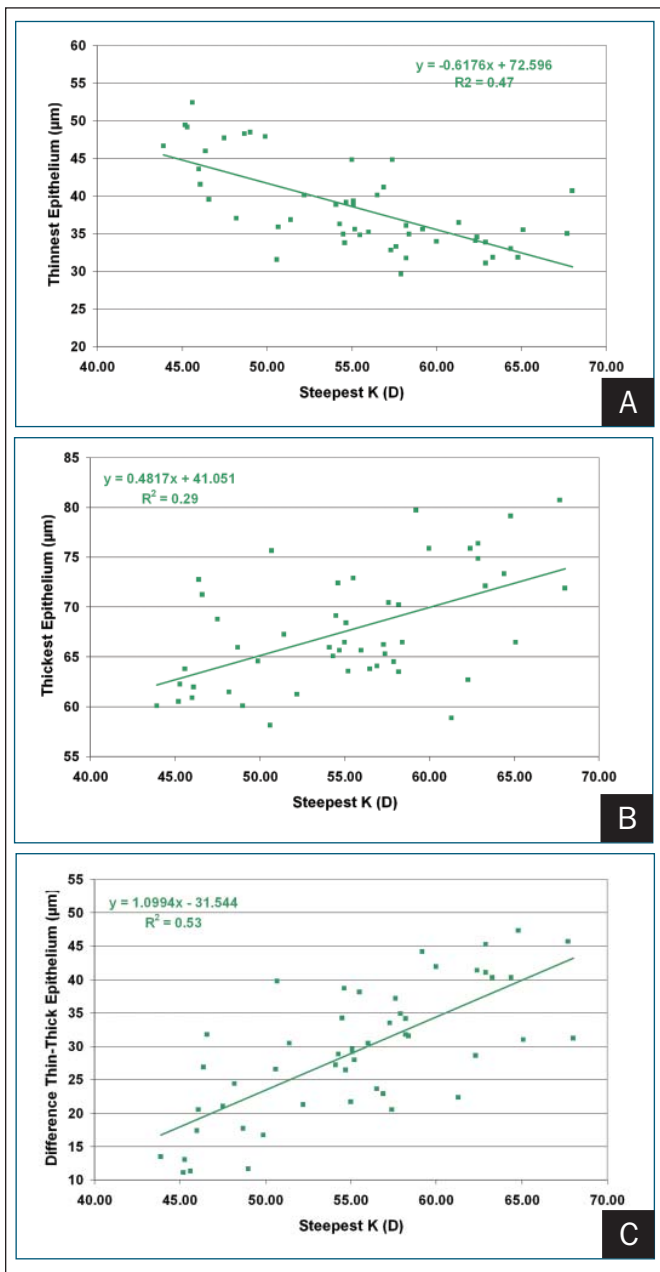


Figure 5. **A)** Correlation between the steepest keratometry (D) and the thinnest epithelium (μm). The coefficient of determination (R^2) is indicated. **B)** Correlation between the steepest keratometry (D) and the thickest epithelium (μm). The coefficient of determination (R^2) is indicated. **C)** Correlation between the steepest keratometry (D) and the difference between the thinnest and thickest epithelium (μm). The coefficient of determination (R^2) is indicated.

the corneal vertex. Table 2 presents statistical data for the average stromal thickness at the thinnest location. The average thinnest stroma was $20.5 \mu\text{m}$ thinner than the average stromal thickness at the corneal vertex, which was a statistically significant difference ($P < .001$). The thinnest stromal point was located in

the inferotemporal quadrant in 51 (94.4%) eyes, in the inferonasal quadrant in 2 (3.7%) eyes, and in the superotemporal quadrant in 1 (1.9%) eye. The thinnest stromal point was not found in the superonasal quadrant for any eyes.

The mean location of the thinnest total corneal point was displaced $0.36 \pm 0.41 \text{ mm}$ temporally and $0.52 \pm 0.36 \text{ mm}$ inferiorly with reference to the corneal vertex. Table 2 presents statistical data for the average total corneal thickness at the thinnest location. The average thinnest total cornea was $22.4 \mu\text{m}$ thinner than the average total corneal thickness at the corneal vertex, which was a statistically significant difference ($P < .001$). The thinnest total corneal point was located in the inferotemporal quadrant in 49 (90.7%) eyes, in the inferonasal quadrant in 3 (5.6%) eyes, and in the superotemporal quadrant in 2 (3.7%) eyes. The thinnest total corneal point was not found in the superonasal quadrant for any eyes.

The maps of stromal and total corneal thickness standard deviation (see Fig 2, rows 2 and 3, column 2) showed the least variation in stromal and total corneal thickness in the superonasal quadrant, and the most variation in the inferotemporal quadrant, around the average thinnest location. Maps of the minimum stromal and total corneal thickness (see Fig 2, rows 2 and 3, column 3) demonstrated the thinnest stroma and total cornea within the study population were slightly decentered inferotemporally, around the average thinnest location. The thinnest central stroma was $298 \mu\text{m}$, whereas the thinnest stroma 3.8 mm superiorly was $450 \mu\text{m}$. The thinnest central total cornea was $338 \mu\text{m}$, whereas the thinnest total cornea 3.8 mm superiorly was $524 \mu\text{m}$. Maps of the maximum stromal and total corneal thickness (see Fig 2, rows 2 and 3, column 4) showed that the thickest stroma and total cornea in the study population were found peripherally at the 3-mm radius in the superonasal cornea. The thickest peripheral stroma was $713 \mu\text{m}$ and the thickest peripheral total cornea was $772 \mu\text{m}$, whereas the thickest central stroma was $490 \mu\text{m}$ and the thickest central total cornea was $541 \mu\text{m}$. Maps of the range of stromal thicknesses (see Fig 2, row 2, column 5) showed that the largest range in stromal thickness in the study population was found in the inferotemporal region around the thinnest point location. Maps of the range of total corneal thicknesses (see Fig 2, row 3, column 5) showed that the largest range in total corneal thickness in the study population was found in the central 3-mm zone.

Figure 7 shows the average and standard deviation stromal thickness maps and total corneal thickness maps calculated for thickness data transposed to center the data on the thinnest point rather than the cor-

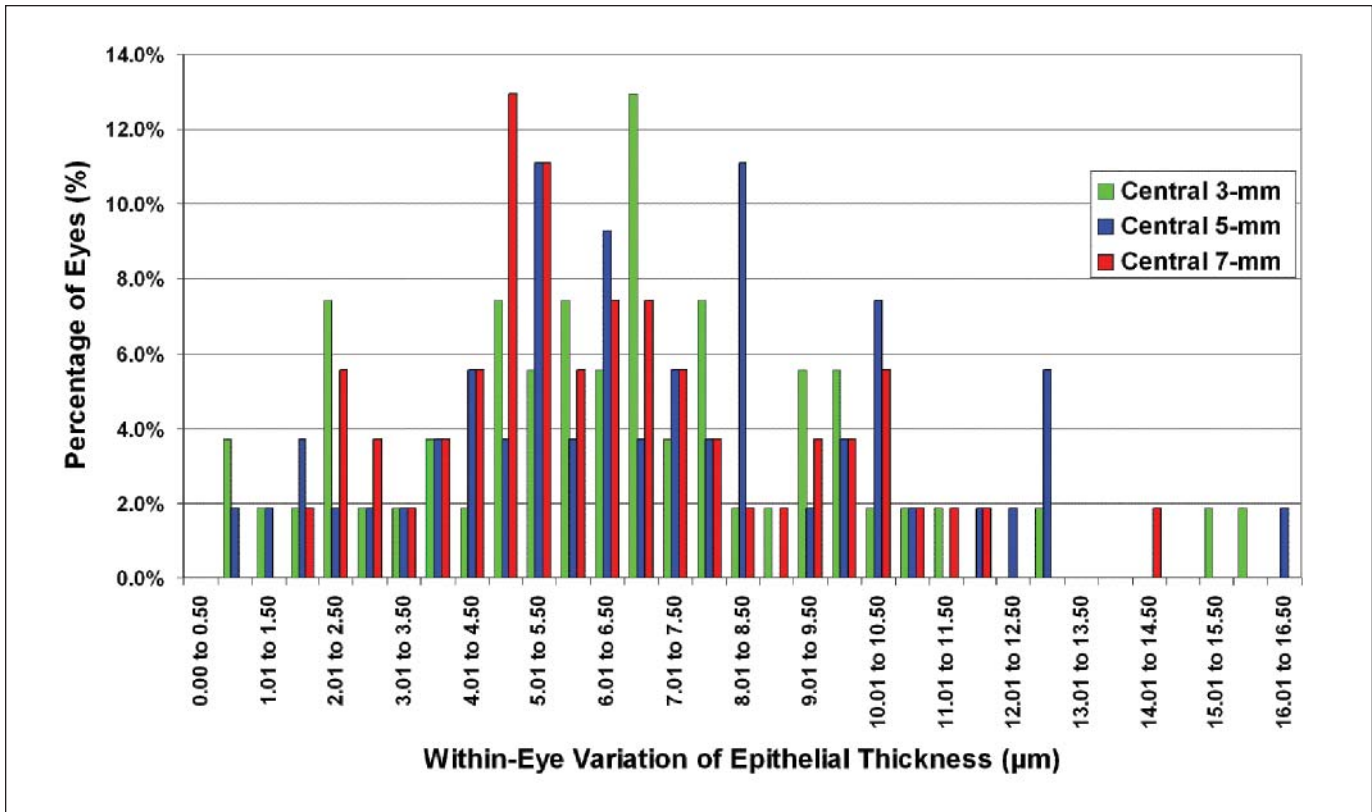


Figure 6. Histogram of within-eye variation of epithelial thickness for the central 3-, 5-, and 7-mm zones. The x axis represents the within-eye variation of epithelial thickness for the central 3-mm (green bars), 5-mm (blue bars), and 7-mm (red bars) diameter zones with intervals of 0.50 μm. Each bar represents the percentage of eyes with the within-eye variation of epithelial thickness for that 0.50 μm interval.

neal vertex. The central thin stromal and total corneal zone appeared to be slightly asymmetrical, extending slightly further towards the periphery superiorly than inferiorly in the vertical meridian. The map of stromal thickness standard deviation showed the least variation in a central zone extending 3 mm nasally and temporally, 1 mm inferiorly, and 2 mm superiorly. The map of total corneal thickness standard deviation showed the least variation in the superior and inferotemporal cornea.

Figure 8 shows the cross-sectional semi-meridional average stromal and total corneal thickness profile for the study population. Figure 9 shows the average absolute stromal and total corneal thickness progression relative to the thinnest stroma and total cornea; the thinnest value is adjusted to zero and the difference between the thinnest value and the thickness at each annular radius is plotted. The average absolute stromal thickness progression can be described by the equation: $y = 2.40 x^2 + 26.367 \times (R^2 = 0.999)$, where y is the absolute difference in stromal thickness (μm) relative to the thinnest point at the x (mm) radius from the thinnest point. The average absolute total corneal thickness progression can be described by the equation: $y = 2.35 x^2 + 31.649 \times (R^2 = 0.999)$. The mean increase

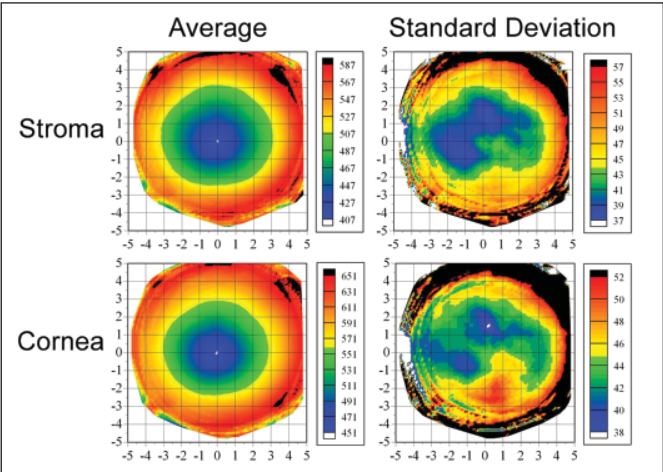


Figure 7. Topographic map of the average and standard deviation of stromal thickness and total corneal thickness for the population centered on the thinnest point. The color scale represents the thickness in microns. A Cartesian 1-mm grid is superimposed with the origin at the thinnest point. Both maps include all eyes with left eyes mirrored (positive x values represent the nasal cornea and negative values mirrored represent the temporal cornea).

in stromal thickness with reference to the thinnest point was $28.5 \pm 15.8 \mu\text{m}$ at the 1-mm radius, $63.7 \pm 23.2 \mu\text{m}$ at the 2-mm radius, and $102.2 \pm 26.6 \mu\text{m}$ at the 3-mm

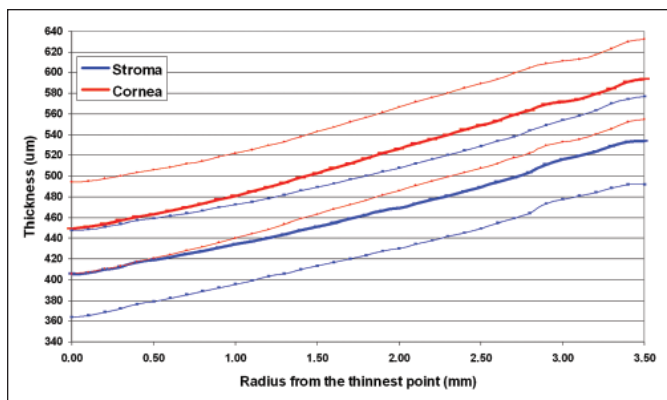


Figure 8. Cross-sectional semi-meridional average stromal and total corneal thickness profile (μm) for all eyes. The data points represent the average thickness of all data within an annulus of a given radius. The x axis is the radial distance (mm) from the location of the thinnest point. The thick line represents the average thickness profile and the thin lines represent one standard deviation less than and one standard deviation greater than the average thickness. The stromal thickness is represented in blue and the total corneal thickness in red.

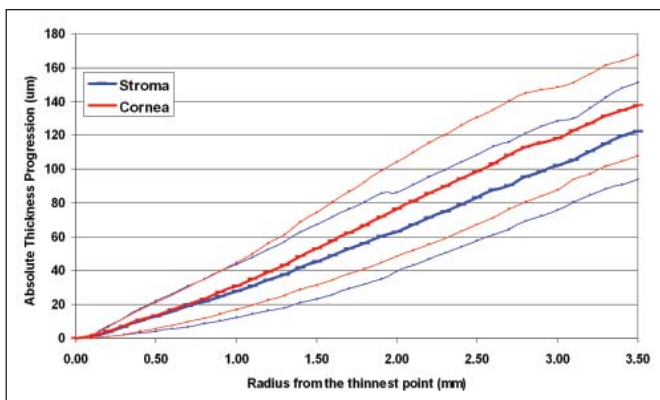


Figure 9. Average absolute stromal and total corneal thickness progression (μm) with reference to the thinnest point for all eyes. The data points represent the difference between the average thickness of all data within an annulus of a given radius and the thinnest thickness. The x axis is the radial distance (mm) from the location of the thinnest point. The thick line represents the absolute thickness progression and the thin lines represent one standard deviation less than and one standard deviation greater than the absolute thickness progression. The stromal thickness is represented in blue and the total corneal thickness in red.

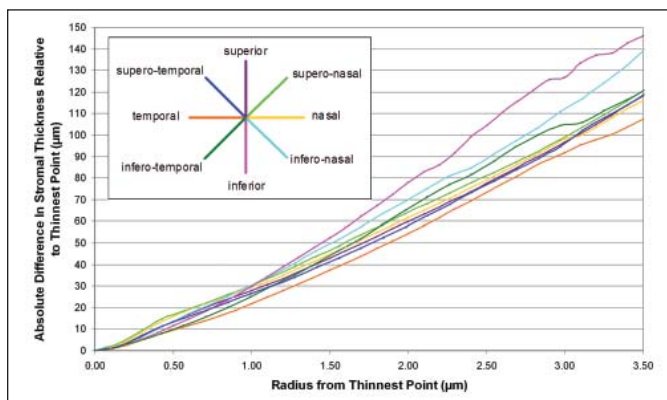


Figure 10. Average absolute stromal thickness progression (μm) with reference to the thinnest point in eight semi-meridians for all eyes using mirrored left eye symmetry. The data points represent the difference between the average stromal thickness of all data within an annulus within a given radius and the value at the thinnest point. The x axis is the radial distance (mm) from the thinnest point location. Each line represents the absolute stromal thickness progression along a given semi-meridian, in eight semi-meridians at 45° intervals.

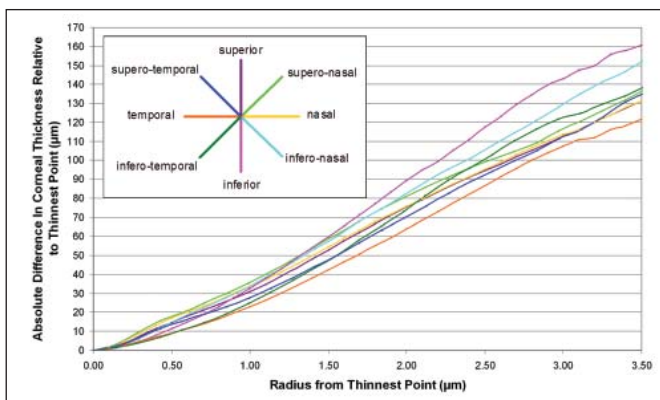


Figure 11. Average absolute total corneal thickness progression (μm) with reference to the thinnest point in eight semi-meridians for all eyes using mirrored left eye symmetry. The data points represent the difference between the average total corneal thickness of all data within an annulus within a given radius and the value at the thinnest point. The x axis is the radial distance (mm) from the thinnest point location. Each line represents the absolute total corneal thickness progression along a given semi-meridian, in eight semi-meridians at 45° intervals.

radius. The mean increase in total corneal thickness with reference to the thinnest point was $30.4 \pm 14.3 \mu\text{m}$ at the 1-mm radius, $75.0 \pm 29.5 \mu\text{m}$ at the 2-mm radius, and $115.7 \pm 34.6 \mu\text{m}$ at the 3-mm radius.

The directional semi-meridional absolute stromal and total corneal thickness progression analysis (Figs 10 and 11) revealed that the rate of increase in stromal and total corneal thickness were greater in the inferior cornea than in the superior cornea and greater in the nasal cornea than the temporal cornea. The nasal and superonasal semi-meridians were thicker than the other semi-meridians within the central 1.2-mm radius zone;

however, the inferior semi-meridian was the thickest from the 1.2-mm radius and further towards the peripheral cornea. The temporal semi-meridian was the thinnest at all radial distances from the thinnest point.

DISCUSSION

This is the first study to characterize the in vivo epithelial, stromal, and total corneal thickness profiles over an area between 6 and 10 mm in diameter in a population of keratoconic eyes. Within the region of the cone, the epithelial thickness profile consisted of a localized zone of thinning surrounded by an annulus

of thickened epithelium. This pattern was characteristic of all keratoconic eyes scanned. We have chosen to describe this specific configuration as an “epithelial doughnut pattern.” At the thinnest location, we found an average epithelial thickness of $38.2 \pm 5.8 \mu\text{m}$, an average stromal thickness of $405.9 \pm 42.5 \mu\text{m}$, and an average total corneal thickness of $449.8 \pm 43.9 \mu\text{m}$. The thinnest epithelial point and the thinnest stromal and total corneal points were displaced on average inferotemporally with reference to the corneal vertex.

It is known that the corneal epithelium has the ability to alter its thickness profile to try and re-establish a smooth, symmetrical optical surface and either partially or totally mask the presence of an irregular stromal surface from front surface topography.²⁷ We have previously described epithelial compensation for stromal irregularities in cases of asymmetric resection in automated lamellar keratoplasty,²⁸ asymmetric LASIK flaps,²⁸⁻³⁰ microfolds,^{29,30} flap malposition,²⁹⁻³¹ short flap,²⁹⁻³¹ free cap malrotation,³² and irregular stromal surface following multiple refractive procedures.²⁷ We have also shown epithelial changes in response to myopic^{22,28,33} and hyperopic LASIK,²⁸ radial keratotomy,³⁴ and Intacs implantation.³⁵

The epithelial doughnut pattern found in all keratoconic eyes in this population is consistent with the known epithelial compensatory mechanism; the epithelium appears to remodel to eliminate or reduce the bulging of the anterior stromal surface and regularize the anterior corneal surface by thinning over the cone and thickening around the cone. We have also shown that the epithelium was both thinner over the cone and thicker around the cone in more advanced cases, indicating that the degree of potential epithelial compensation is dependent on the severity of the keratoconus.

We originally suggested in 1994 that eyelid blinking and friction onto the corneal surface may regulate the epithelial thickness profile²⁶ and have recently suggested that eyelid mechanics and blinking might be responsible for the non-uniform epithelial thickness profile seen in normal corneas.²⁴ We postulated that the eyelid might effectively be chafing the surface epithelium during blinking and that the posterior surface of the semi-rigid tarsus provides a template for the outer shape of the epithelial surface. In keratoconus, because the cone is protruding, the apex would be the first point of contact with the eyelid, resulting in increased chafing and therefore thinning of the epithelium at the apex of the cone. As the cone becomes more severe and the protrusion becomes more pronounced, it makes sense that the epithelium at the apex of the cone becomes thinner. We have indeed found that the thinnest epithelium in the central zone of the epithelial doughnut pattern was thinner for

eyes with steeper keratometry (more advanced keratoconus) (see Fig 5A). This is also visibly apparent on the B-scans presented in Figure 1. The epithelial response to the insertion of intracorneal ring segments provides a similar example of this phenomenon; the epithelium becomes thinner where the intracorneal ring segment causes a ridge in the anterior stromal surface.³⁵ Further study is required to confirm our theory that the eyelid is effectively chafing the epithelium causing epithelial thinning over a stromal cone.

As the cone becomes more severe, we have also shown that the surrounding annulus of epithelium in the epithelial doughnut pattern is thicker (see Fig 5B). The presence of annular epithelial thickening suggests that the eyelid is applying less force during blinking around the sides of the cone, allowing the epithelium to grow up to the inner surface template of the eyelid; in a sense, the eyelid inner surface is tented over the apex of a bulging cone, producing lateral valleys, which are then filled with thickened epithelium. Again, this epithelial reaction is exactly the same as that seen after intracorneal ring segments; the epithelium is thicker to the side of the ridge caused by the intracorneal ring segment as the epithelium has been allowed to grow into the space created by the tenting effect of the eyelid over the ridge.³⁵ The epithelial reaction can be thought of in terms of draping a cloth sheet over an irregular surface with the edges pulled taut. A taut cloth would not lie evenly across the surface; rather, it would be in contact with the peaks of the irregular surface and tent-shaped above the surface on either side of the peaks before gradually returning to the surface in areas without irregularities. The anterior surface of the cornea can be seen to be similar to such a tent-shape in the B-scans in Figure 1. Further study is required to confirm our theory that the reduced eyelid force around a cone allows the epithelium to thicken.

The combination of epithelial thinning and surrounding epithelial thickening resulted in an increased difference between the thinnest and thickest epithelium; as the cone became more severe, the difference between the thinnest and thickest epithelium increased (see Fig 5C).

The difference between the thinnest and thickest epithelium showed a stronger correlation with the steepest keratometry than the thinnest epithelium or thickest epithelium alone. This is not surprising as this parameter combines the impact of both the epithelial thinning and thickening effects. In our population, the difference between the thinnest and thickest epithelium reached $59 \mu\text{m}$ in the most advanced case. This describes how the degree of epithelial compensatory reaction is associated with the severity of the cone.

These factors demonstrate that the epithelial thick-

ness profile changes with the progression of the disease. We propose that parameters such as epithelial thickness at the thinnest point (at the center of the epithelial doughnut pattern) and maximum thickness difference between the localized central zone of thinning (at the center of the epithelial doughnut pattern) and the surrounding annulus of thick epithelium could be used to monitor the progression and severity of keratoconus. Localized thinning of the epithelium at the center of the epithelial doughnut pattern and an increased difference between the thinnest and thickest epithelium might indicate deterioration of the condition.

Having previously characterized the epithelial thickness profile in a population of normal eyes,²⁴ we know that the epithelial thickness profile in keratoconus has a significantly different pattern. Additionally, we have demonstrated that the epithelial thickness profile in keratoconus changes as the disease progresses. Therefore, we can assume that the epithelial doughnut pattern would be observed in early keratoconus, where the degree of epithelial thickness changes would be expected to be relatively small. We are currently investigating the possibility of using epithelial thickness profiles as a screening tool for early detection of keratoconus.³⁶

Comparing our results with previous studies, it was reported that the average corneal vertex epithelial thickness in keratoconus was $48.2 \pm 5.5 \mu\text{m}$ and the average cone apex epithelial thickness was $6.1 \mu\text{m}$ thinner ($42.1 \pm 4.5 \mu\text{m}$) when using OCT.⁵ This is in good agreement with our findings; in our population, the epithelial thickness at the thinnest location was $7.5 \mu\text{m}$ thinner than at the corneal vertex. Our findings both at the corneal vertex and at the thinnest locations were slightly lower than that reported by Haque et al.⁵ This difference could be easily explained by variations in the severity of the keratoconus witnessed in the sample population. Haque et al's study also demonstrated that patients who had been diagnosed more than 5 years prior to the assessment had an apical epithelium $2.6 \mu\text{m}$ thinner than patients diagnosed more recently.⁵ This is in agreement with our finding that the thinnest epithelium at the center of the epithelial doughnut pattern was thinner for more advanced cases.

We have previously characterized the stromal thickness profile and absolute stromal thickness progression in a population of normal eyes.²⁴ Comparing this to the average absolute stromal thickness progression reported in the present study for a keratoconic population, there is a significant difference to that observed in normal eyes. In normal eyes, we demonstrated that the absolute stromal thickness progression from the thinnest point to the periphery showed little variation between eyes and that it was independent of central stromal thickness.²⁴ In

keratoconus, the absolute stromal thickness progression from the thinnest point to the periphery showed greater variation between eyes and was much faster than that in the normal population. For example, at a 2-mm radius from the thinnest point, the stromal thickness progression in normal eyes was $29.9 \pm 5.4 \mu\text{m}$ whereas it was $60.6 \pm 25.6 \mu\text{m}$ in keratoconus. The increased difference between stromal thickness at the thinnest point and in the periphery in the keratoconus population indicates central thinning. This difference could be observed in early cases of keratoconus, and therefore absolute stromal thickness progression might be a sensitive tool for keratoconus detection.

This is the first published study to describe the characteristics of epithelial, stromal, and total corneal pachymetric topography in the keratoconic cornea. Thickness mapping of the corneal epithelium demonstrated an epithelial doughnut pattern characterized by localized central thinning surrounded by an annulus of thickened epithelium. The epithelial doughnut pattern was more pronounced in eyes with more advanced keratoconus. Knowledge of epithelial, stromal, and total corneal thickness profiles in keratoconus may help in the diagnosis of early keratoconus, as well as the monitoring of the progression of the disease under therapeutic conditions such as corneal collagen cross-linking,^{37,38} where the surface topography changes may not reflect the stromal surface changes due to masking by epithelial remodeling.²⁷

AUTHOR CONTRIBUTIONS

Study concept and design (D.Z.R., T.J.A., R.H.S., D.J.C.); data collection (D.Z.R., T.J.A.); interpretation and analysis of data (D.Z.R., M.G., T.J.A., R.H.S., D.J.C.); drafting of the manuscript (D.Z.R., M.G., T.J.A.); critical revision of the manuscript (D.Z.R., M.G., T.J.A., R.H.S., D.J.C.); statistical expertise (T.J.A.)

REFERENCES

1. Gromacki SJ, Barr JT. Central and peripheral corneal thickness in keratoconus and normal patient groups. *Optom Vis Sci.* 1994;71:437-441.
2. Gherghel D, Hosking SL, Mantry S, Banerjee S, Naroo SA, Shah S. Corneal pachymetry in normal and keratoconic eyes: Orbscan II versus ultrasound. *J Cataract Refract Surg.* 2004;30:1272-1277.
3. Owens H, Watters GA. An evaluation of the keratoconic cornea using computerised corneal mapping and ultrasonic measurements of corneal thickness. *Ophthalmic Physiol Opt.* 1996;16:115-123.
4. De Sanctis U, Missolungi A, Mutani B, Richiardi L, Grignolo FM. Reproducibility and repeatability of central corneal thickness measurement in keratoconus using the rotating Scheimpflug camera and ultrasound pachymetry. *Am J Ophthalmol.* 2007;144:72-718.
5. Haque S, Simpson T, Jones L. Corneal and epithelial thickness in keratoconus: a comparison of ultrasonic pachymetry, Orbscan II, and optical coherence tomography. *J Refract Surg.* 2006;22:486-493.

6. Kawana K, Miyata K, Tokunaga T, Kiuchi T, Hiraoka T, Oshika T. Central corneal thickness measurements using Orbscan II scanning slit topography, noncontact specular microscopy, and ultrasonic pachymetry in eyes with keratoconus. *Cornea*. 2005;24:967-971.
7. Auffarth GU, Wang L, Volcker HE. Keratoconus evaluation using the Orbscan topography system. *J Cataract Refract Surg*. 2000;26:222-228.
8. Liu Z, Zhang M, Chen J, Luo L, Chen L, Gong X, Huang T, Lin Y, Wang Z. Corneal topography and thickness in keratoconus [Chinese]. *Zhonghua Yan Ke Za Zhi*. 2002;38:740-743.
9. Emre S, Doganay S, Yologlu S. Evaluation of anterior segment parameters in keratoconic eyes measured with the Pentacam system. *J Cataract Refract Surg*. 2007;33:1708-1712.
10. Ambrosio R Jr, Alonso RS, Luz A, Coca Velarde LG. Corneal-thickness spatial profile and corneal-volume distribution: tomographic indices to detect keratoconus. *J Cataract Refract Surg*. 2006;32:1851-1859.
11. Avitabile T, Marano F, Uva MG, Reibaldi A. Evaluation of central and peripheral corneal thickness with ultrasound biomicroscopy in normal and keratoconic eyes. *Cornea*. 1997;16:639-644.
12. Avitabile T, Marano F, Castiglione F, Reibaldi A. Keratoconus staging with ultrasound biomicroscopy. *Ophthalmologica*. 1998;212:10-12.
13. Haque S, Fonn D, Simpson T, Jones L. Corneal and epithelial thickness changes after 4 weeks of overnight corneal refractive therapy lens wear, measured with optical coherence tomography. *Eye Contact Lens*. 2004;30:189-193.
14. Luz A, Ursulio M, Castañeda D, Ambrósio R Jr. Corneal thickness progression from the thinnest point to the limbus: study based on a normal and a keratoconus population to create reference values [Portuguese]. *Arq Bras Oftalmol*. 2006;69:579-583.
15. Mohamed S, Lee GK, Rao SK, Wong AL, Cheng AC, Li EY, Chi SC, Lam DS. Repeatability and reproducibility of pachymetric mapping with Visante anterior segment-optical coherence tomography. *Invest Ophthalmol Vis Sci*. 2007;48:5499-5504.
16. Mandell RB, Polse KA. Keratoconus: spatial variation of corneal thickness as a diagnostic test. *Arch Ophthalmol*. 1969;82:182-188.
17. Avitabile T, Franco L, Ortisi E, Castiglione F, Pulvirenti M, Torrisi B, Castiglione F, Reibaldi A. Keratoconus staging: a computer-assisted ultrabiomicroscopic method compared with videokeratographic analysis. *Cornea*. 2004;23:655-660.
18. Kaya V, Karakaya M, Utine CA, Albayrak S, Oge OF, Yilmaz OF. Evaluation of the corneal topographic characteristics of keratoconus with orbscan II in patients with and without atopy. *Cornea*. 2007;26:945-948.
19. Scroggs MW, Proia AD. Histopathological variation in keratoconus. *Cornea*. 1992;11:553-559.
20. Aktekin M, Sargon MF, Cakar P, Celik HH, Firat E. Ultrastructure of the cornea epithelium in keratoconus. *Okajimas Folia Anat Jpn*. 1998;75:45-53.
21. Hayes S, Boote C, Tuft SJ, Quantock AJ, Meek KM. A study of corneal thickness, shape and collagen organisation in keratoconus using videokeratography and X-ray scattering techniques. *Exp Eye Res*. 2007;84:423-434.
22. Reinstein DZ, Silverman RH, Trokel SL, Coleman DJ. Corneal pachymetric topography. *Ophthalmology*. 1994;101:432-438.
23. Reinstein DZ, Silverman RH, Raevsky T, Simoni GJ, Lloyd HO, Najafi DJ, Rondeau MJ, Coleman DJ. Arc-scanning very high-frequency digital ultrasound for 3D pachymetric mapping of the corneal epithelium and stroma in laser in situ keratomileusis. *J Refract Surg*. 2000;16:414-430.
24. Reinstein DZ, Archer TJ, Gobbe M, Silverman RH, Coleman DJ. Epithelial thickness in the normal cornea: three-dimensional display with Artemis very high-frequency digital ultrasound. *J Refract Surg*. 2008;24:571-581.
25. Reinstein D, Archer T, Gobbe M, Silverman R, Coleman DJ. Stromal thickness in the normal cornea: three-dimensional display with Artemis very high-frequency digital ultrasound. *J Refract Surg*. Available at: www.journalofrefractive surgery.com/preprint.asp. Posted online September 30, 2008.
26. Reinstein DZ, Silverman RH, Coleman DJ. High-frequency ultrasound measurement of the thickness of the corneal epithelium. *Refract Corneal Surg*. 1993;9:385-387.
27. Reinstein DZ, Archer T. Combined Artemis very high-frequency digital ultrasound-assisted transepithelial phototherapeutic keratectomy and wavefront-guided treatment following multiple corneal refractive procedures. *J Cataract Refract Surg*. 2006;32:1870-1876.
28. Reinstein DZ, Silverman RH, Sutton HF, Coleman DJ. Very high-frequency ultrasound corneal analysis identifies anatomic correlates of optical complications of lamellar refractive surgery: anatomic diagnosis in lamellar surgery. *Ophthalmology*. 1999;106:474-482.
29. Reinstein DZ, Silverman RH. Artemis VHF digital ultrasound technology. In: Wang M, ed. *Corneal Topography in the Wavefront Era*. Thorofare, NJ: SLACK Incorporated; 2006:207-225.
30. Reinstein DZ, Archer TJ. Very high-frequency digital ultrasound: Artemis 2 scanning in corneal refractive surgery. In: Vinciguerra P, Camesasca FI, eds. *Refractive Surface Ablation: PRK, LASEK, Epi-LASIK, Custom, PTK and Retreatment*. Thorofare, NJ: SLACK Incorporated; 2006:315-330.
31. Reinstein DZ, Archer TJ, Silverman RH. Evaluation of irregular astigmatism with Artemis very high-frequency digital ultrasound scanning. In: Wang M, ed. *Irregular Astigmatism: Diagnosis and Treatment*. Thorofare, NJ: SLACK Incorporated; 2007:29-42.
32. Reinstein DZ, Rothman RC, Couch DG, Archer TJ. Artemis very high-frequency digital ultrasound-guided repositioning of a free cap after laser in situ keratomileusis. *J Cataract Refract Surg*. 2006;32:1877-1883.
33. Reinstein D, Srivannaboon S, Gobbe M, Archer T, Silverman R, Sutton H, Coleman DJ. Epithelial thickness profile changes induced by myopic LASIK as measured by Artemis very high-frequency digital ultrasound. *J Refract Surg*. Available at: <http://www.journalofrefractive surgery.com/preprint.asp>. Posted online October 15, 2008.
34. Lovisolo CF, Mularoni A, Calossi A. Complications of refractive keratotomy. In: Alio J, Azar DT, eds. *Management of Complications in Refractive Surgery*. Berlin, Germany: Springer-Verlag; 2008:197-224.
35. Reinstein DZ, Srivannaboon S, Holland SP. Epithelial and stromal changes induced by intacs examined by three-dimensional very high-frequency digital ultrasound. *J Refract Surg*. 2001;17:310-318.
36. Reinstein DZ, Archer TJ, Gobbe M. Corneal epithelial thickness profile in the diagnosis of keratoconus. *J Refract Surg*. In press.
37. Wollensak G, Spoerl E, Seiler T. Riboflavin/ultraviolet-a-induced collagen crosslinking for the treatment of keratoconus. *Am J Ophthalmol*. 2003;135:620-627.
38. Reinstein DZ, Carp G, Archer TJ, Gobbe M. VHF digital ultrasound scanning observations after corneal cross linking. Presented at: International Congress of Corneal Cross Linking; December 8-9, 2006; Zurich, Switzerland.